



# Stellar Variability at the Main-sequence Turnoff of the Intermediate-age LMC Cluster NGC 1846\*

R. Salinas<sup>1</sup> , M. A. Pajkos<sup>2,7</sup>, A. K. Vivas<sup>3</sup> , J. Strader<sup>4</sup> , and R. Contreras Ramos<sup>5,6</sup>

<sup>1</sup> Gemini Observatory, Casilla 603, La Serena, Chile; [rsalinas@gemini.edu](mailto:rsalinas@gemini.edu)

<sup>2</sup> Department of Physics and Astronomy, Butler University, Indianapolis, IN 46208, USA

<sup>3</sup> Cerro Tololo Interamerican Observatory, National Optical Astronomy Observatory, Casilla 603, La Serena, Chile

<sup>4</sup> Department of Physics and Astronomy, Michigan State University, East Lansing, MI 48824, USA

<sup>5</sup> Millennium Institute of Astrophysics, Av. Vicuña Mackenna 4860, 782-0436 Macul, Santiago, Chile

<sup>6</sup> Instituto de Astrofísica, Pontificia Universidad Católica de Chile, Av. Vicuña Mackenna 4860, 782-0436 Macul, Chile

Received 2017 December 6; revised 2018 February 19; accepted 2018 February 22; published 2018 April 5

## Abstract

Intermediate-age (IA) star clusters in the Large Magellanic Cloud (LMC) present extended main-sequence turn-offs (MSTO) that have been attributed to either multiple stellar populations or an effect of stellar rotation. Recently it has been proposed that these extended main sequences can also be produced by ill-characterized stellar variability. Here we present Gemini-S/Gemini Multi-Object Spectrometer (GMOS) time series observations of the IA cluster NGC 1846. Using differential image analysis, we identified 73 new variable stars, with 55 of those being of the Delta Scuti type, that is, pulsating variables close the MSTO for the cluster age. Considering completeness and background contamination effects, we estimate the number of  $\delta$  Sct belonging to the cluster between 40 and 60 members, although this number is based on the detection of a single  $\delta$  Sct within the cluster half-light radius. This amount of variable stars at the MSTO level will not produce significant broadening of the MSTO, albeit higher-resolution imaging will be needed to rule out variable stars as a major contributor to the extended MSTO phenomenon. Though modest, this amount of  $\delta$  Sct makes NGC 1846 the star cluster with the highest number of these variables ever discovered. Lastly, our results present a cautionary tale about the adequacy of shallow variability surveys in the LMC (like OGLE) to derive properties of its  $\delta$  Sct population.

**Key words:** globular clusters: individual (NGC 1846) – Magellanic Clouds – stars: variables: delta Scuti

**Supporting material:** data behind figure, machine-readable table

## 1. Introduction

Intermediate-age (IA) star clusters in the Large Magellanic Cloud (LMC) exhibit extended main-sequence turn-offs (MSTOs) inconsistent with single stellar populations (Mackey & Broby Nielsen 2007; Mackey et al. 2008; Milone et al. 2009), which cannot be explained by photometric errors, contamination from the LMC field, or binaries (e.g., Goudfrooij et al. 2009). These extended MSTOs can be interpreted as two bursts of star formation separated by a few hundred Myr or a continuous star formation lasting a similar amount of time (Mackey & Broby Nielsen 2007). This interpretation, however, is complicated because any age spread at the MSTO level should also be visible at the red clump, but the morphology of red clumps is rather consistent with single stellar populations (Li et al. 2014; Bastian & Niederhofer 2015, but see Goudfrooij et al. 2015 for a different viewpoint). Moreover, for younger clusters with ages of a few Myr, where any extended star formation should be even clearer in their color–magnitude diagrams (CMDs), the evidence of departures from single stellar populations remains highly debated (Bastian & Silva-Villa 2013; Correnti et al. 2015; Niederhofer et al. 2015; Milone et al. 2017).

An alternative explanation could be given by stellar rotation. Fast-rotating stars with ages  $\sim 1.5$  Gyr, will have different temperatures as a function of latitude. When viewed from different angles, these temperature differences will be seen as a range of colors and luminosities, producing an extension to the MSTO, mimicking the effect of multiple stellar populations (Bastian & de Mink 2009; Yang et al. 2013; Brandt & Huang 2015). However, it has been claimed that rotation alone cannot fully reproduce the extended MSTO morphology (Girardi et al. 2011; Goudfrooij et al. 2017).

Recently, Salinas et al. (2016b) have shown that another previously overlooked factor must be considered to understand these extended MSTOs. The instability strip will cross the upper MS and MSTO area for clusters with ages between 1 and 3 Gyr, and therefore a certain number of the stars within the instability strip will develop pulsations. These main-sequence pulsators are known as Delta Scuti stars (hereafter  $\delta$  Sct, see e.g., Breger 2000, for a review). For CMDs obtained using single images per filter, as the great majority of CMDs derived from *HST* images (Mackey & Broby Nielsen 2007; Mackey et al. 2008; Milone et al. 2009), as well as most of the ground-based observations (e.g., Piatti et al. 2014), the act of observing these variables at a random phase means their magnitudes and colors will be away from their static values, producing an artificial broadening of the MSTO that can be misinterpreted as the effect of an extended star formation history or rotation.

The impact of variables near the MSTO will depend on the percentage of stars developing pulsations (the incidence) and on the magnitude of the pulsation amplitudes. These factors are very poorly constrained in extragalactic systems. In Carina, for

\* Based on observations obtained at the Gemini Observatory, which is operated by the Association of Universities for Research in Astronomy, Inc., under a cooperative agreement with the NSF on behalf of the Gemini partnership: the National Science Foundation (United States), the National Research Council (Canada), CONICYT (Chile), Ministerio de Ciencia, Tecnología e Innovación Productiva (Argentina), and Ministério da Ciência, Tecnologia e Inovação (Brazil).

<sup>7</sup> CTIO/Gemini REU student.

example, Vivas & Mateo (2013) find a lower limit of 8% for the incidence and an amplitude distribution with a peak at  $A_V \sim 0.5$  mag.

The properties of these quantities in the LMC clusters are even less constrained. That is the case because it is difficult to detect them. First, they are faint stars. With magnitudes between 20 and 22 at the LMC distance, they are out of reach of most of the large variability surveys, which are conducted with small-aperture telescopes. Second, their periods are short, which has the consequence that the exposure times must kept short to correctly sample the light curve. At least medium size telescopes are then needed.

A quick revision through the catalog of  $\delta$  Sct in the LMC of Poleski et al. (2010) reveals that for the 14 IA clusters listed in Piatti et al. (2014), between zero and two  $\delta$  Sct are found per cluster, indicating that crowding significantly hampers the reliability of OGLE at these faint magnitudes, and only a handful of  $\delta$  Sct have been found in other searches (e.g., Kaluzny & Rucinski 2003).

### 1.1. The IA Cluster NGC 1846

NGC 1846 (R.A. = 05:07:34.9, decl. =  $-67:27:32.45$ ) is a rather massive ( $M = 1.25 \times 10^5 M_\odot$ ; Baumgardt et al. 2013), IA ( $\sim 2$  Gyr; Mackey & Broby Nielsen 2007), and metal-rich ( $[\text{Fe}/\text{H}] = -0.49$ ; Grocholski et al. 2006) LMC cluster. It was the first LMC cluster where an extended and bifurcated MSTO was detected and firmly established (Mackey & Broby Nielsen 2007; Mackey et al. 2008; Goudfrooij et al. 2009), and where explanations involving field contamination and binary evolution were discarded as a cause (Goudfrooij et al. 2009).

With a core radius of  $\sim 6.5$  pc (Keller et al. 2011), NGC 1846 is also one of the most extended IA clusters, which makes it a more suitable candidate for ground-based photometry. Large core radii have been suggested to be associated with the presence of extended MSTOs (Keller et al. 2011).

We assess the role of  $\delta$  Sct in the morphology of the MSTO in IA clusters in the LMC using new time series imaging of the LMC cluster NGC 1846.

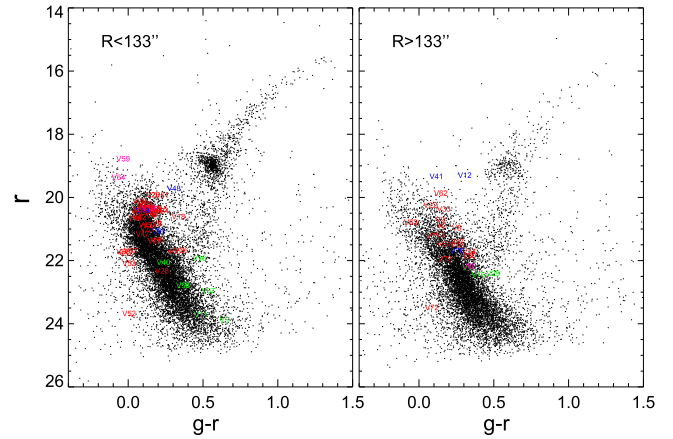
## 2. Observations and Data Reduction

Observations of NGC 1846 were conducted using the 8.1 m Gemini South telescope, located at Cerro Pachón, Chile, on the night of 2015 December 30 under the Gemini Fast Turnaround mode (Gemini program GS-2015B-FT-7). The imaging mode of the Gemini Multi-Object Spectrometer (GMOS; Hook et al. 2004) provided us a 5.5 square arcminute field of view (fov). The SDSS filter system was used to yield 6, 66, and 6 images, in  $g$ ,  $r$ , and  $i$ , each having exposure times of 120 s, 120 s, and 90 s, respectively. The total time span of observations was 0.136 days (3.26 hr), adequate for detection of  $\delta$  Sct, which will have periods of less than  $\sim 6$  hr. The GMOS-S array detector consists of three  $2048 \times 4176$  pixels Hamamatsu detectors, each separated by a gap  $\sim 30$  pixels wide. Observations were obtained with  $2 \times 2$  binning, resulting in a pixel scale of  $0''.16 \text{ pixel}^{-1}$ .

Raw data retrieved from the Gemini Observatory Archive<sup>8</sup> were reduced using the GEMINI package in IRAF.<sup>9</sup> Specifically,

<sup>8</sup> <https://archive.gemini.edu>

<sup>9</sup> IRAF is distributed by the National Optical Astronomy Observatories, which are operated by the Association of Universities for Research in Astronomy, Inc., under cooperative agreement with the National Science Foundation.



**Figure 1.** GMOS photometry of the NGC 1846 field. The left panel shows the inner  $133''$  from the cluster center, while the right panel shows the area outside this limit out to the edges of the GMOS fov. The  $133''$  limit defines equal areas within the fov. Variable stars discovered in the field are colored according to their classification: delta Scuti (red), RR Lyrae (blue), eclipsing (green), and unknown classification (magenta). The inner population of  $\delta$  Sct is more than double the population of the outer field.

the GMOS subpackage allowed us to bias and flatfield correct the raw images, as well as mosaic the chips and trim their overscan region. Image quality was measured with the GEMSEED task. The median FWHM for the  $r$  data set was  $0''.8$ .

### 2.1. Photometry

Photometry of the images was obtained using the DAOPHOT/ALLSTAR/ALLFRAME suite of programs developed by Stetson (1987, 1994). As a first step, DAOPHOT was run over all images. The preliminary positions and aperture-photometry magnitudes were used to obtain the coordinate transformations between the frames with the help of DAOMATCH/DAOMASTER (Stetson 1993). Close to 50 bright isolated stars were visually chosen on the best seeing image of each filter to model the psf as a linearly varying Gaussian profile. The same psf stars were used in the rest of the frames transforming the coordinates using the DAOMASTER output. Once psf photometry was obtained for all images with ALLSTAR, a deep reference frame was constructed using the 20 best seeing images. This reference frame was used to obtain the positions of the stars to be measured by ALLFRAME (Stetson 1994), which fits simultaneously the PSF to all stars in all of the available images. Final catalogs with mean instrumental magnitudes in  $g$ ,  $r$ , and  $i$  measured by ALLFRAME were obtained with DAOMASTER.

Given the absence of standards stars taken on the night of the observations, calibration to the standard system was achieved using the transformation equations provided by the observatory for the Hamamatsu CCDs.<sup>10</sup>

The CMD of the NGC 1846 field can be seen in Figure 1. This diagram has further cleaning steps leaving only stars with ALLSTAR parameters  $\chi < 10$  and  $-2 < \text{sharp} < 2$  and photometric errors less than 0.1 mag in each filter. Photometry of the field is shown split in two equal areas. The left panel shows the inner area ( $R < 133''$ ), where the MSTO of the cluster can be seen at  $r \sim 21$  and  $g-r \sim 0.15$ , and also evidence for old, intermediate and young populations on the LMC field. The subgiant branch of NGC 1846 is barely

<sup>10</sup> <https://www.gemini.edu/?q=node/10445>

distinguishable at  $r \sim 20$  and  $0.2 < g - r < 0.5$ . The right panel shows the surrounding field of  $R > 133''$ . Here, the IA MSTO and red clump are less pronounced and even though a young and IA population still exist, the dominant feature is the old LMC population, whose MSTO is around  $r = 23$ . The image quality of ground-based observations does not permit one to see the double MSTO, which is clearly seen with *HST* observations (e.g., Mackey & Broby Nielsen 2007; Milone et al. 2009).

### 3. Variable Stars in NGC 1846

#### 3.1. Known Variables

We searched for the known variables in the cluster using the on-line search tool provided by OGLE.<sup>11</sup> OGLE lists 44 variables within the fov observed with GMOS. Of these, 39 are classified as long-period variables, 4 as RR Lyrae (RRL), and 1 as Cepheid (Soszyński et al. 2009a, 2009b). No short-period variables were found in this cluster by OGLE. Given the age of the cluster, any RRL or Cepheid will not be a member of the cluster but members of the LMC field.

#### 3.2. Searching for New Variables

New variables stars in the NGC 1846 field were searched using the image subtraction package ISIS (v 2.1, Alard 2000). ISIS first registers images to a common astrometric system. Then a reference frame is constructed as a median from the best seeing images. This reference is then convolved to match the psf of the rest of the images. Once the psf is matched, the subtraction is applied. This approach leaves in principle only the variable sources as residuals in these subtracted images. ISIS also constructs a variance image as the mean of absolute normalized deviations. This variance image is then visually inspected for meaningful variations in order to discard spurious artifacts produced, for example, around saturated stars (e.g., Salinas et al. 2016a). ISIS finally makes psf photometry on the selected positions where variability is suspected, giving as output light curves in fluxes relative to the reference frame. Variable sources were searched in the  $r$  data set that had the higher cadence of observations. Relative flux light curves are transformed into magnitudes following the procedure from Catelan et al. (2013). Periodicity in the light curves was searched using the phase dispersion minimization algorithm (Stellingwerf 1978) as implemented in IRAF, using 0.001 and 0.3 days as limiting periods.

#### 3.3. Variable Star Classification

The visual inspection of the variance image produced 164 candidate variable sources. Of this initial list, after a careful visual inspection of the light curves, we settled on 76 genuine varying sources in the NGC 1846 field covered by GMOS (Figure 2). Two of these were not detected by DAOPHOT in either the  $g$  nor the  $r$  filters due to crowding, and therefore their light curves could not be transformed to magnitudes. Additionally, three more were only detected in the better quality  $r$  data. Our final classification, based on the colors, magnitudes, periods, shapes of the light curve, and amplitudes of each source, yields a result of 55  $\delta$  Sct, 8 eclipsing binaries,

5 RRL stars (3 of them already detected by OGLE), and 7 sources with no clear classification.

Table 1 gives positions, periods, and intensity-weighted magnitudes for all of these variables. Given the short time span of the observations, for many variables only a lower limit for the period is provided. Phased light curves can be seen in Figures 7–10. Additionally, Figure 11 gives light curves for the candidate and known RRL stars in the field in Julian date versus magnitude. The Appendix also gives notes for some of the variables, especially those with some ambiguity in their classification.

#### 3.4. Period and Amplitude Distribution

Figure 3 shows the period and amplitude distribution for 48  $\delta$  Sct in NGC 1846 where both quantities have been measured, together with the same quantities for 937  $\delta$  Sct in the LMC from Poleski et al. (2010). Both distributions were obtained using an adaptive kernel density estimator (Epanechnikov 1969).

The period distribution of  $\delta$  Sct in NGC 1846 (left panel) has a peak at  $\sim 0.06$  day and a tail toward longer periods. The secondary peak around at  $\sim 0.13$  day is an artifact arising from the time span of the observations, where this lower limit was assigned for  $\delta$  Sct with longer periods (see Table 1). The peak of the period distribution from Poleski et al. (2010) is slightly higher, 0.08 day, but significant. The percentage of  $\delta$  Sct in NGC 1846 with  $P < 0.05$  day is 20% while in the Poleski et al. (2010) sample this is only 0.2%. The scarcity of these short-period  $\delta$  Sct in the Poleski et al. (2010) sample may indicate that the cadence of OGLE observations, close to 3 days (Poleski et al. 2010), is inadequate to find them.

The amplitude distribution of  $\delta$  Sct in NGC 1846 has its peak around 0.03 mag with a tail toward larger amplitudes up to 0.4 mag. Even though the OGLE data gives amplitudes in the  $I$  filter instead of  $r$ , it is obvious that the amplitude distribution in the LMC field is very different to the one in NGC 1846. OGLE observations are most likely severely missing a large part of the  $\delta$  Sct in the LMC field.

### 4. The Influence of Delta Scuti in the MSTO Morphology

The position of each variable in a CMD can be seen in Figure 1. As expected,  $\delta$  Sct clusters around the IA MSTOs of the cluster and the field population, with a few along the upper main sequence, and another group that are probably background  $\delta$  Sct. Field RRL appear as slightly brighter and redder than the IA TO. The faintness of RRL is partly because all their light curves miss the maximum, making their mean magnitudes dimmer.

Figure 2 in Salinas et al. (2016b) shows that hundreds or even thousands of  $\delta$  Sct would be needed to produce a significant broadening of the MSTO in IA clusters.

In order to compare with the predictions of Salinas et al. (2016b), we need to estimate the total number of  $\delta$  Sct in the cluster.

#### 4.1. Artificial Stars and Completeness

To know how many detections we are missing given crowding and the image quality, we set up a standard artificial stars experiment using the task `addstar` within DAOPHOT. We added 45000 artificial stars (in 30 independent runs to avoid overcrowding) with magnitudes between  $25 < r < 15$ , whose  $g - r$  colors and luminosity function were extracted

<sup>11</sup> <http://ogledb.astrouw.edu.pl/~ogle/CVS/>

**Table 1**  
Positions, Mean Magnitudes,  $r$  Amplitudes, Periods, and Classification for All of the Variables Discovered in the NGC 1846 Field

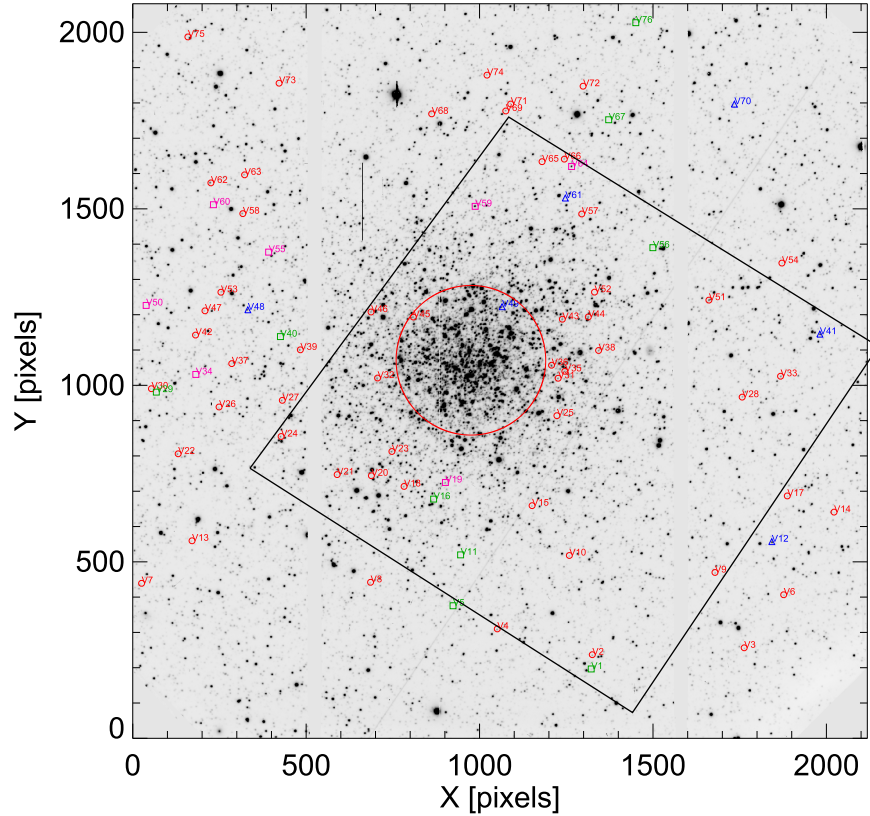
ID	R.A. (J2000)	Decl. (J2000)	$\langle g \rangle$	$\langle r \rangle$	$A_r$	$P(\text{day})$	Type	Note
V1	05:07:10.061	-67:28:34.35	22.60	22.31	0.31	0.17	E	*
V2	05:07:11.184	-67:28:34.85	21.10	20.98	0.03	0.042	D	
V3	05:07:11.684	-67:29:44.91	21.37	21.26	0.02	0.043	D	
V4	05:07:13.242	-67:27:51.07	20.78	20.66	0.02	0.076	D	
V5	05:07:15.079	-67:27:30.68	24.58	23.97	0.32	0.13	E	*
V6	05:07:15.856	-67:30:03.18	21.27	21.05	0.03:	0.14	D	
V7	05:07:16.925	-67:25:07.09	21.35	21.30	0.10	0.060	D	
V8	05:07:16.946	-67:26:52.67	21.06	20.90	0.04	0.064	D	
V9	05:07:17.633	-67:29:31.52	20.90	20.79	0.03	0.075	D	
V10	05:07:19.007	-67:28:24.38	21.57	21.42	0.02	0.052	D	
V11	05:07:19.084	-67:27:34.23	24.23	23.79	0.25:	>0.15	E	
V12	05:07:20.048	-67:29:57.74	19.64	19.38	0.10:	>0.2	RRL	OGLE-LMC-RRLYR-05278
V13	05:07:20.256	-67:25:30.38	21.80	21.59	0.08	0.042	D	
V14	05:07:22.364	-67:30:26.48	22.09	21.80	0.03	0.15	D	
V15	05:07:22.941	-67:28:07.24	21.02	20.95	0.04	0.076	D	
V16	05:07:23.480	-67:27:21.83	22.44	22.01	0.18	0.13	D	
V17	05:07:23.651	-67:30:04.94	21.69	21.48	0.03	0.054	D	
V18	05:07:24.485	-67:27:08.23	20.98	20.69	0.03	0.14	D	
V19	05:07:24.787	-67:27:27.30	20.51	20.42	0.04:	>0.14	U	*
V20	05:07:25.334	-67:26:53.16	20.12	20.00	0.02	0.1	D	
V21	05:07:25.431	-67:26:37.37	21.59	21.46	0.05	0.10	D	
V22	05:07:27.099	-67:25:24.06	20.36	20.33	0.03:	0.12	D	
V23	05:07:27.237	-67:27:02.63	20.35	20.28	0.04	0.068	D	
V24	05:07:28.438	-67:26:11.55	20.69	20.51	0.03:	0.10	D	
V25	05:07:30.025	-67:28:18.75	...	...	...	0.13	E	*
V26	05:07:30.772	-67:25:42.96	22.07	21.76	0.06	0.046	D	
V27	05:07:31.283	-67:26:12.13	20.49	20.46	0.01	0.044	D	
V28	05:07:31.454	-67:29:44.21	22.59	22.41	0.09	0.046	D	
V29	05:07:31.953	-67:25:14.02	22.94	22.49	0.12:	>0.12	E	
V30	05:07:32.221	-67:25:11.77	22.22	21.93	0.08	0.15	D	
V31	05:07:32.974	-67:28:19.35	20.51	20.42	0.02	0.074	D	
V32	05:07:33.023	-67:26:56.07	20.55	20.43	0.04	0.078	D	
V33	05:07:33.096	-67:30:01.91	20.57	20.45	0.20:	0.11	D	
V34	05:07:33.336	-67:25:32.26	...	24.09	0.25	0.12	U	*
V35	05:07:33.519	-67:28:22.44	20.57	20.44	0.08	0.12	D	
V36	05:07:34.001	-67:28:16.31	20.24	20.21	0.02	0.078	D	
V37	05:07:34.180	-67:25:48.84	21.74	21.77	0.13	0.14	D	
V38	05:07:35.155	-67:28:38.01	20.70	20.59	0.03	0.125	D	
V39	05:07:35.255	-67:26:20.48	20.39	20.33	0.02	0.071	D	
V40	05:07:36.298	-67:26:11.30	22.33	22.14	0.10	0.14	E	
V41	05:07:36.410	-67:30:20.05	19.49	19.42	0.07:	>0.16	RRL	OGLE-LMC-RRLYR-05379
V42	05:07:36.430	-67:25:32.14	20.73	20.70	0.02	0.038	D	
V43	05:07:37.626	-67:28:21.32	20.63	20.50	0.02	0.095	D	
V44	05:07:37.799	-67:28:33.29	20.47	20.39	0.10	0.075	D	
V45	05:07:37.816	-67:27:12.63	20.63	20.46	0.03	0.104	D	
V46	05:07:38.220	-67:26:53.09	20.74	20.74	0.04	0.071	D	
V47	05:07:38.335	-67:25:36.50	21.29	21.24	0.08:	>0.20	D	
V48	05:07:38.412	-67:25:56.26	20.06	19.80	0.08:	>0.16	RRL	OGLE-LMC-RRLYR-05394
V49	05:07:38.618	-67:27:53.52	20.55	20.50	0.16:	>0.2	RRL	*
V50	05:07:38.767	-67:25:09.38	...	24.44	0.50	0.10	U	*
V51	05:07:39.109	-67:29:28.91	20.20	20.02	0.02	0.15	D	
V52	05:07:39.754	-67:28:36.16	23.72	23.76	0.40	0.071	D	*
V53	05:07:39.796	-67:25:43.87	22.13	22.17	0.15	0.16	D	*
V54	05:07:42.020	-67:30:02.59	21.68	21.56	0.02	0.049	D	
V55	05:07:42.945	-67:26:05.89	...	23.42	0.50:	>0.1	U	*
V56	05:07:43.251	-67:29:03.09	23.19	22.87	0.25:	>0.15	E	*
V57	05:07:45.914	-67:28:30.28	21.80	21.86	0.05	0.049	D	*
V58	05:07:45.974	-67:25:53.99	20.51	20.47	0.03	0.11	D	
V59	05:07:46.526	-67:27:41.14	18.78	18.86	0.01	>0.16	U	*
V60	05:07:46.679	-67:25:40.43	22.55	22.26	0.11	>0.10	U	*
V61	05:07:47.170	-67:28:22.70	21.31	21.15	0.80:	>0.2	RRL	*
V62	05:07:48.396	-67:25:39.26	20.05	19.95	0.11	0.09	D	
V63	05:07:49.025	-67:25:54.81	20.77	20.87	0.12	0.07	D	
V64	05:07:49.655	-67:28:25.60	19.34	19.45	0.01:	>0.16	U	*

**Table 1**  
(Continued)

ID	R.A. (J2000)	Decl. (J2000)	$\langle g \rangle$	$\langle r \rangle$	$A_r$	$P(\text{day})$	Type	Note
V65	05:07:50.038	-67:28:11.99	22.05	21.79	0.06	>0.16	D	
V66	05:07:50.236	-67:28:22.26	20.57	20.55	0.01	0.047	D	
V67	05:07:53.337	-67:28:42.72	23.53	23.04	0.35	0.11	E	
V68	05:07:53.811	-67:27:21.08	21.72	21.80	0.12:	>0.16	D	*
V69	05:07:54.035	-67:27:55.26	20.65	20.54	0.02	0.127	D	
V70	05:07:54.560	-67:29:40.68	21.98	21.77	0.12:	>0.2	RRL	*
V71	05:07:54.581	-67:27:57.52	21.16	21.08	0.02	0.067	D	
V72	05:07:55.982	-67:28:30.90	23.61	23.57	0.34	0.128	D	*
V73	05:07:56.233	-67:26:10.71	22.16	22.03	0.05	0.15	D	
V74	05:07:56.857	-67:27:46.59	21.06	20.96	0.02	0.057	D	
V75	05:07:59.875	-67:25:28.64	...	...	...	0.095	D	*
V76	05:08:00.985	-67:28:55.19	22.88	22.53	0.12:	>0.18	E	

**Note.** Uncertain amplitudes are indicated with a colon, while the > indicates lower limits for some periods. The classification is D: Delta Scuti, RRL: RR Lyrae, E: eclipsing binary, LP: long-period variable, and U: variable with unknown classification. The last column indicates either a cross identification with OGLE or a note in the [Appendix](#) indicated with the \* symbol.

(This table is available in machine-readable form.)

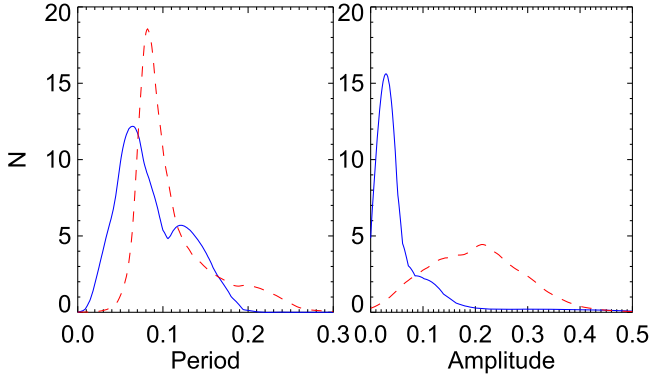


**Figure 2.** A finder chart for variables in the NGC 1846 field based on a GMOS  $r$  image. North is up and east is to the left. Positions of  $\delta$  Sct are indicated with red circles, RRL with blue triangles, and eclipsing binaries with green squares. Magenta squares mark the position of variables of unknown type. The central large red circle represents the half-light radius from Goudfrooij et al. (2009). The fov of GMOS is approximately  $5.5 \times 5.5$  arcmin, while the large black square indicates the HST/ACS pointing used by Goudfrooij et al. (2009) and Milone et al. (2009). North is up and east is to the left.

from an IA synthetic CMD produced using BaSTI models (Pietrinferni et al. 2004). Stars were spatially distributed mimicking the distribution in the field, with two-thirds of the stars in each run randomly distributed and one-third with a Gaussian distribution around the cluster center. Once the photometry over the frames with the added stars was complete, artificial stars were considered as recovered if they lied within two pixels from their input positions and if the magnitude

difference between output and input magnitudes was less than 0.5 mag.

As seen in Figure 4, completeness is greatly compromised in the inner  $\sim 50''$ , affecting at the 50% level the  $20 < r < 21.5$  mag range where most of the  $\delta$  Sct lie. The completeness is close to 90% for stars outside  $\sim 120''$  in the same magnitude range. Lines represent the same interpolating function used in, e.g., Salinas et al. (2015).



**Figure 3.** Period (left panel) and amplitude (right panel) distribution of  $\delta$  Sct in NGC 1846 (blue solid lines) compared to  $\delta$  Sct in the LMC field from Poleski et al. (2010) (red dashed lines). Note that Poleski et al. (2010) amplitudes are in  $I$  while our amplitudes are in  $r$ . The bump in the period distribution is an artifact produced by time span limit of the observations.

#### 4.2. Scaling to the Total Number

Once we know how many  $\delta$  Sct we are missing as function of radius, we need to use this information to estimate the number of  $\delta$  Sct in the inner parts of the cluster where the completeness is poor. To this end, we assume the incidence of  $\delta$  Sct will not vary with radius, and that  $\delta$  Sct follow the same radial distribution as the bright stars that dominate the overall light distribution; that is, there should be no significant mass segregation between the RGB stars and the upper MS stars, given their mass difference of less than  $\sim 15\%$ . The absence of a strong mass segregation between upper MS stars and RGB stars in NGC 1846 is confirmed by the analysis of Goudfrooij et al. (2009) based on *HST* data.

Goudfrooij et al. (2009) fit the radial distribution of stars in NGC 1846 with a King (1962) profile

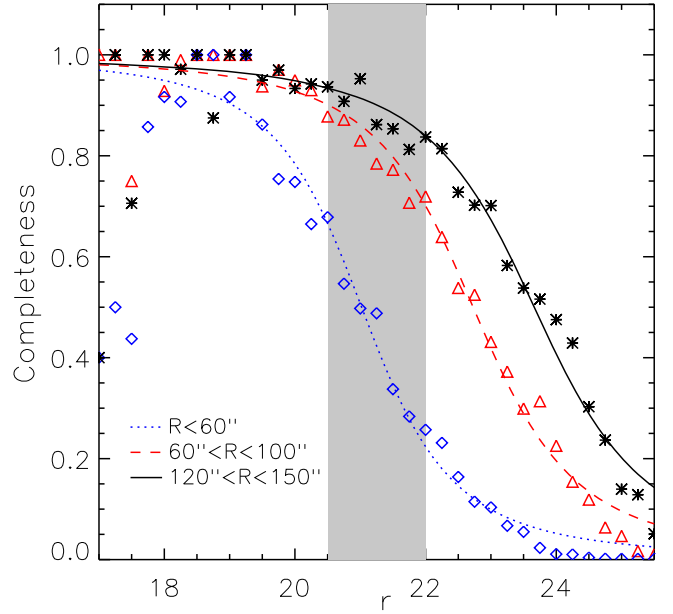
$$n(r) = n_0 \left( \frac{1}{\sqrt{1 + (r/r_c)^2}} - \frac{1}{\sqrt{1 + c^2}} \right)^2 + \text{bkg} \quad (1)$$

finding best fit-parameters  $n_0 = 8.1$ ,  $r_c = 26''$ ,  $c = 6.2$  and  $\text{bkg} = 0.267$ .

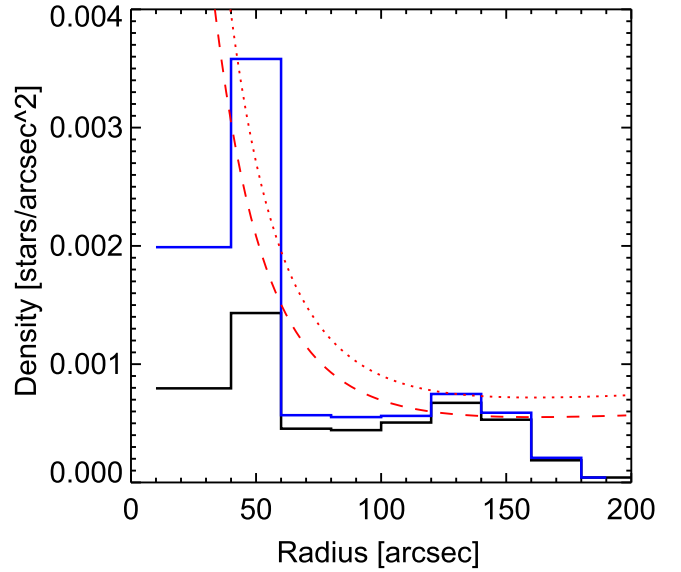
Under the assumption that  $\delta$  Sct follows the distribution of light, we can scale this profile to find a total number of  $\delta$  Sct. We use the  $120'' < R < 140''$  range to define the normalization of the King profile for the  $\delta$  Sct. From the completeness experiment (Section 4.1), a 90% completeness for  $\delta$  Sct is expected at this distance. In this annulus, there are 11 detected  $\delta$  Sct. We integrate the King profile between these limits and that find a normalization factor of 0.0269 gives the expected number of 12.2  $\delta$  Sct in the annulus. Integrating now the King profile from 0 to the tidal radius ( $\sim 200''$ , Goudfrooij et al. 2009), we obtain 150  $\delta$  Sct, where 90 would correspond to the background and 60 would be cluster members.

This number is sensitive to the choice of annulus. If we select instead the  $100'' < R < 120''$  range (where we are approximately 80% complete), the same exercise gives us a total number of 45  $\delta$  Sct members, which indicates that extrapolations, given our severe inner incompleteness, are necessarily very uncertain. Both King profiles can be seen in Figure 5.

Another uncertainty comes from the background level. Structural parameters of NGC 1846 measured by Goudfrooij et al. (2009) using ACS data might overestimate the background given the limited fov of the ACS. If we assume 90% of



**Figure 4.** Results from the artificial stars experiment. The different symbols show the completeness at different cluster-centric annuli. The gray stripe highlights the approximate magnitude range that  $\delta$  Sct will occupy at the cluster's distance.



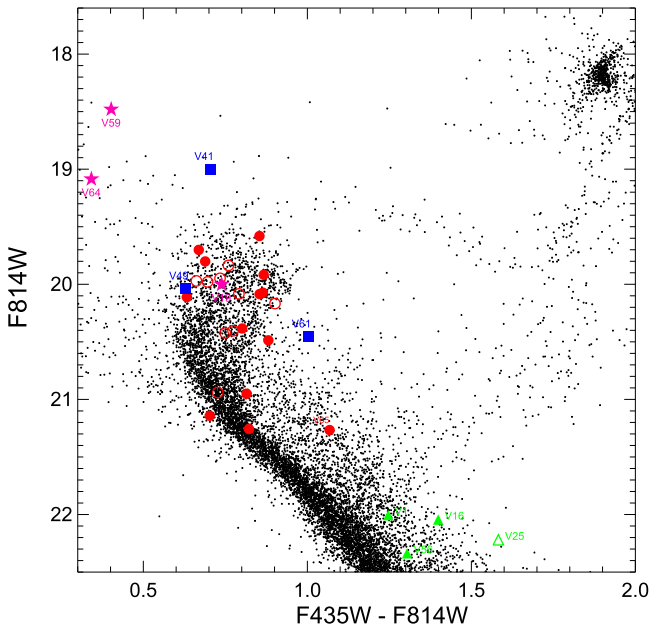
**Figure 5.** Radial distribution of the discovered  $\delta$  Sct. The black solid line shows the detected distribution, while the blue line shows the corrected distribution based on the completeness test. The dashed and dotted lines represent the scaled King profiles as described in the text. The estimated numbers for field and cluster  $\delta$  Sct come from the integration of these King profiles.

the background given by Goudfrooij et al. (2009), then the total number of  $\delta$  Sct increases to a range between 50 and 65. At 70% of the background, this range increases to 62 and 84.

#### 4.3. A Comparison with *HST* Photometry

Even though the total estimated number of discovered  $\delta$  Sct and, in general, the low amplitudes found are most likely not enough to produce any significant broadening of the MSTO, it is interesting to see what impact these discovered  $\delta$  Sct have in the published *HST* photometry.

We cross-matched the F435W/F814W *HST*/ACS photometry of NGC 1846 from Milone et al. (2009) to the positions



**Figure 6.** *HST* photometry of NGC 1846 from Milone et al. (2009) zoomed in the MSTO and upper MS area. Thirty-three of the 36 variable stars found in this paper within the ACS fov are shown. Open symbols represent variables with poor quality photometry as defined in Milone et al. (2009), while filled symbols are variables with good measurements. Red symbols are  $\delta$  Sct, blue symbols are RRL, green symbols are eclipsing binaries, and magenta symbols are variables with undefined class. For clarity, only a few  $\delta$  Sct discussed in the main text are labeled.

of our discovered variables. Given the much smaller ACS fov, only 35 of the discovered variables are found within this fov; 25 being  $\delta$  Sct. These can be seen as red symbols in Figure 6. Catalogs were matched using a combination of CATACOMB<sup>12</sup> and STILTS (Taylor 2006).

Just like in the case of the GMOS photometry (Figure 1), variables stars concentrate at the MSTO. Figure 6 shows the ACS photometry of the upper MS and MSTO areas where 32 of the discovered variables stars are. Open symbols are stars with poorly measured photometry according to Milone et al. (2009) based on the frame-to-frame scatter (see below), uncertainty in the frame-to-frame position and the residual of the psf fit.

One notable feature is that  $\delta$  Sct do not lie preferentially along any of the split sequences but instead scatter along both and with a slightly larger range in color, as expected for variable stars caught at a random phase.

The Milone et al. (2009) ACS photometry of NGC 1846 comes from three exposures in F435W and four in F814W. Despite that Milone et al. (2009) applied a selection based on the rms of the magnitudes in different exposures to set up the good quality sample, 24 out of the 35 variables were labeled as good quality by them, including all 3 RRL, which are expected to have the largest rms based on their larger amplitudes. This again proves the inadequacy of using poorly time-sampled data, as is the case for all IA LMC clusters observed with *HST*, in order to detect variable stars.

## 5. Summary and Conclusions

In this paper, we explored the influence the  $\delta$  Sct pulsators have in the morphology of the MSTO in IA clusters in the LMC. As the great majority of the photometry of these clusters comes

from using merely 1 or 2 images per filter (e.g., Mackey & Broby Nielsen 2007; Milone et al. 2009; Piatti et al. 2014), these variables have so far being undetected and their role ignored.

Using new time series photometry of the LMC IA cluster NGC 1846 obtained with Gemini South, we have discovered 55  $\delta$  Sct in the field of NGC 1846, plus 18 variables of other types. This is the first in-depth study of the short-period variables in an LMC cluster. Considering completeness and background contamination, we estimate the number of  $\delta$  Sct belonging to the cluster to be somewhere around 40 and 60. This number of  $\delta$  Sct will not produce a significant impact in the MSTO morphology, as hundreds or even thousands would be needed to produce a significant broadening of the MSTO according to the modeling of Salinas et al. (2016b).

This estimated total number of  $\delta$  Sct is still very uncertain. We assumed the radial distribution of  $\delta$  Sct follows the light of the cluster to extrapolate the density of  $\delta$  Sct to the inner radii where crowding makes measurements impossible. Moreover, we detected only one  $\delta$  Sct within the half-light radius, where a large number of variables should still be uncovered. Only time-series observations with higher spatial resolution will provide the final answer to the role  $\delta$  Sct have in the broadening of MSTOs.

Finally, we note that NGC 1846 is, to our knowledge, the star cluster with the largest population of  $\delta$  Sct ever discovered, including open clusters in our Galaxy (e.g., Andersen et al. 2009; Sandquist et al. 2016). This opens new avenues for the study of PL relations of  $\delta$  Sct, for example, as function of metallicity, which will be studied in a forthcoming paper. The fact that we have discovered more than 50 of these variables in a patch of the sky where OGLE detected none is a warning that OGLE is most probably severely incomplete for fields with only mild crowding and very biased toward variables with long periods and large amplitudes; therefore, probably thousands of  $\delta$  Sct, fainter, mostly eclipsing variables and even some RRL located in the distant edge of the LMC remain to be discovered.

R.S. thanks Antonino Milone for making his *HST*/ACS photometry of NGC 1846 available and Ernst Paunzen for pointing us to the Galactic clusters richest in  $\delta$  Sct. We thank Catherine Kaleida for all of her efforts organizing the REU program at CTIO. This project was conducted in the framework of the CTIO REU Program, which is supported by the National Science Foundation under grant AST-1062976. J.S. acknowledges partial support from NSF grant AST-1308124 and the Packard Foundation. Based on observations made with the NASA/ESA *Hubble Space Telescope*, and obtained from the Hubble Legacy Archive, which is a collaboration between the Space Telescope Science Institute (STScI/NASA), the Space Telescope European Coordinating Facility (ST-ECF/ESA), and the Canadian Astronomy Data Centre (CADC/NRC/CSA).

*Facility:* Gemini-S.

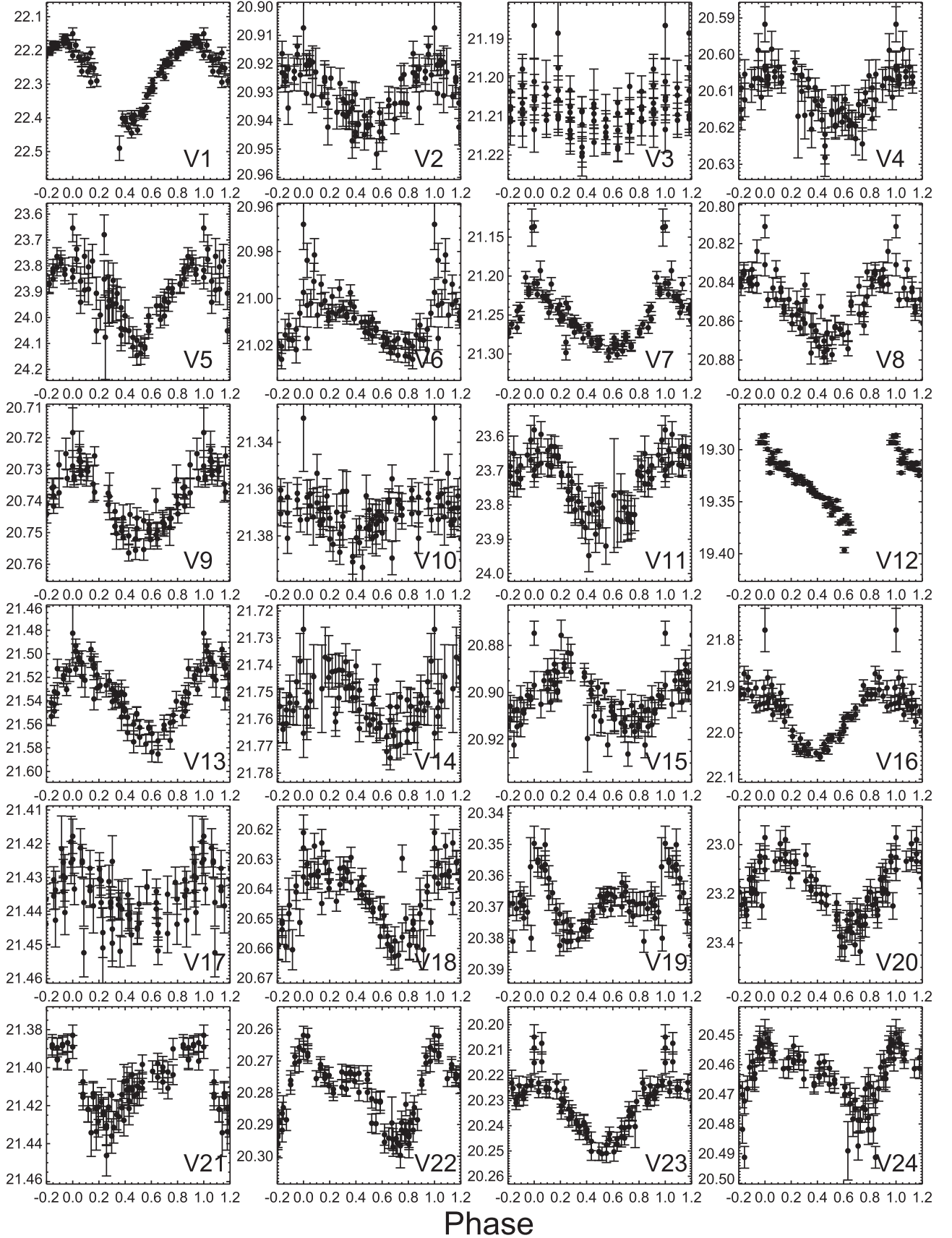
*Software:* IRAF (Tody 1986, 1993), ISIS (v 2.1, Alard 2000), CataComb, stilts (Taylor 2006), daophot/allstar/allframe (Stetson 1987, 1994), daomatch/daomaster (Stetson 1993).

## Appendix

### Notes on Some Individual Variables

V1: even though this could easily be an eclipsing variable at the MSTO of the old LMC population, its curve at maximum light also resembles an RRc variable.

<sup>12</sup> Developed by Paolo Montegriffo at the Bologna Astronomical Observatory.



**Figure 7.** Folded light curves of all of the new variables stars in the NGC 1846 field. All light curves were measured in the  $r$  band. Note that a couple of them (V25 and V75) were not calibrated into standard magnitudes, and their light curves are only shown in relative counts. Variables where only a minimum period is given in Table 1 were phased using this minimum period. The data used to create this figure are available.

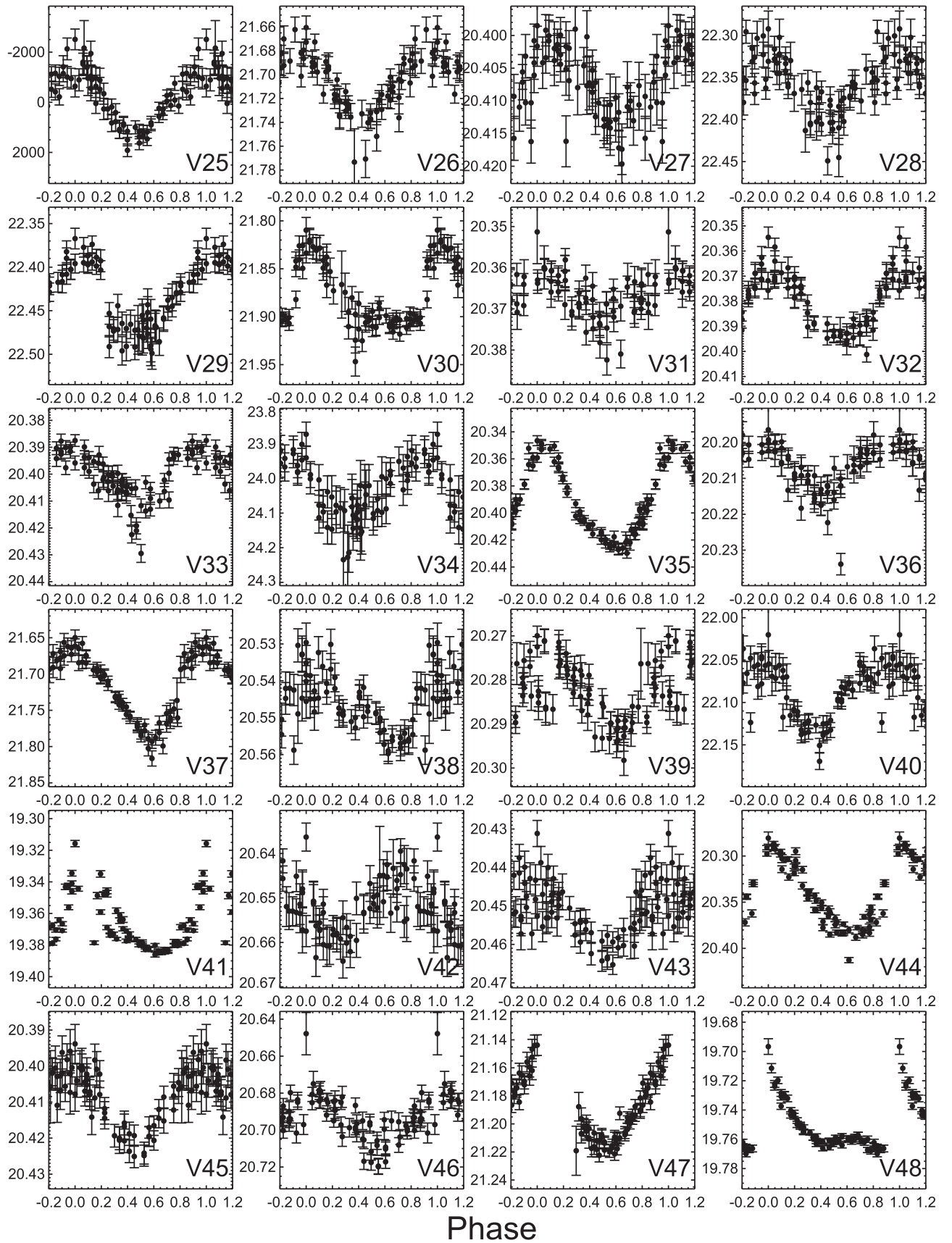


Figure 8. Same as in Figure 7.

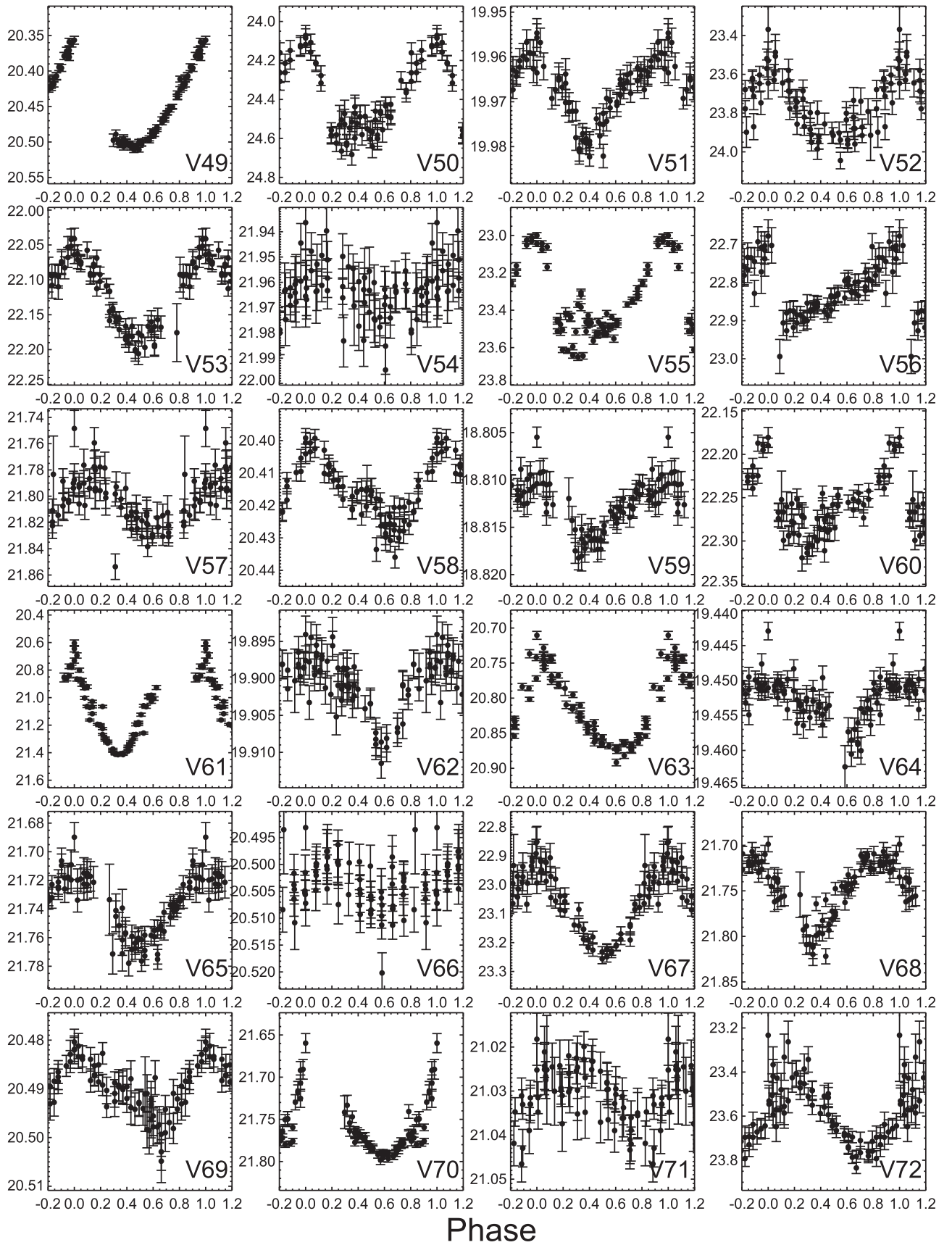


Figure 9. Same as in Figure 7.

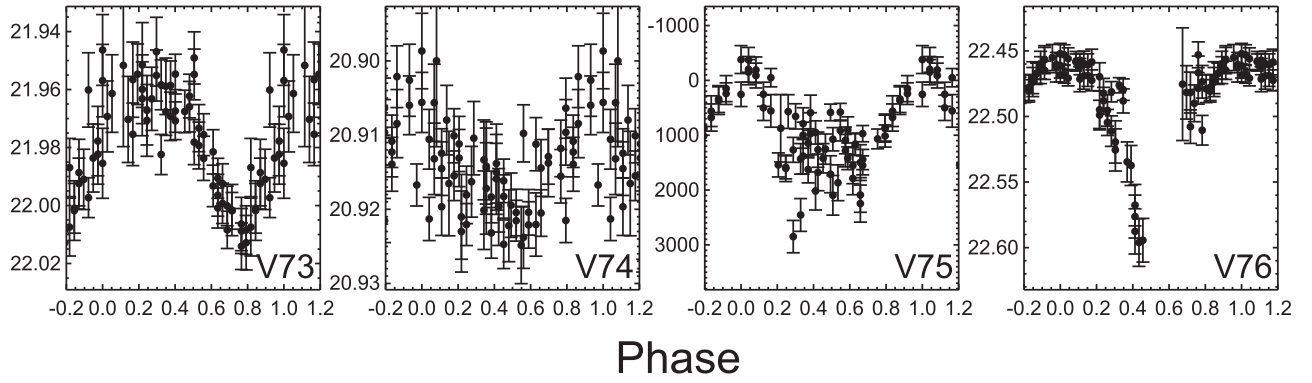


Figure 10. Same as in Figure 7.

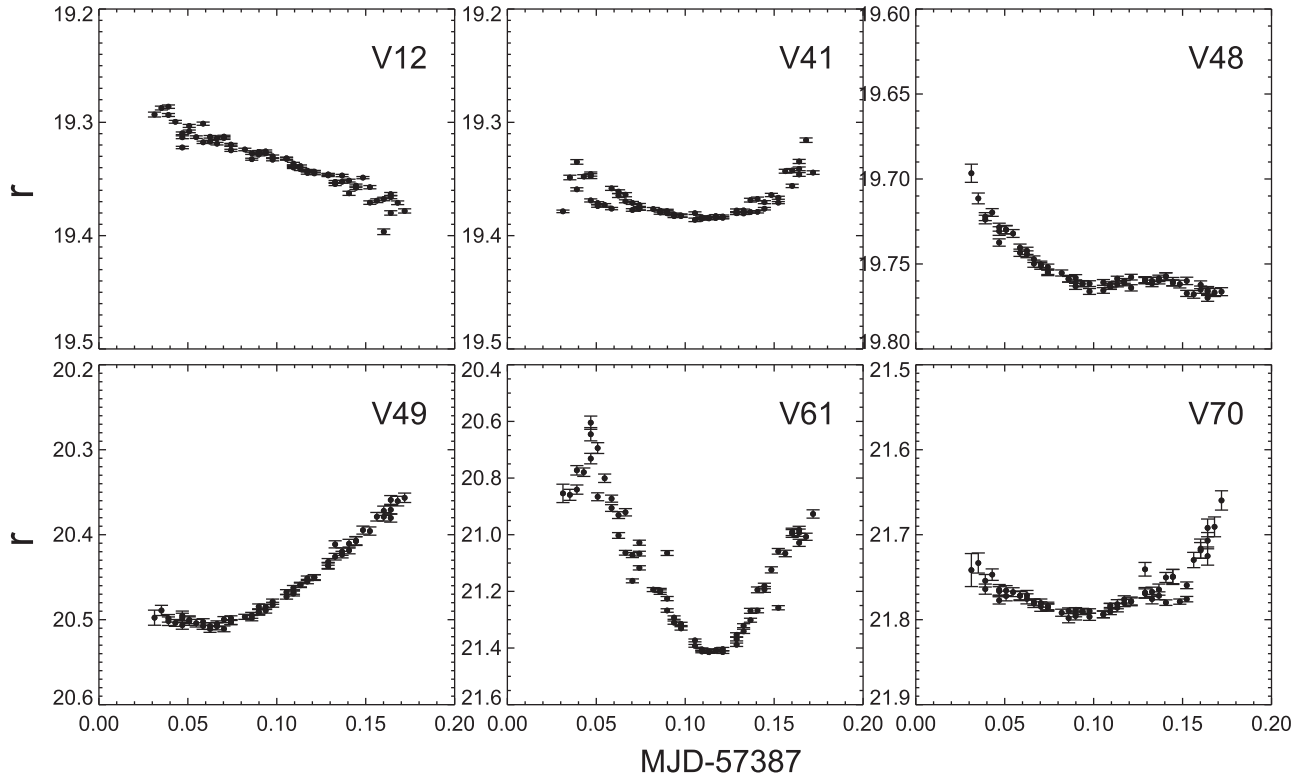


Figure 11. Known RRL (top row) discovered by OGLE and new candidate RRL (bottom row). Light curves are given in modified Julian date vs. magnitude.

V5: by its color and luminosity is most probably an MS contact binary, although its shape looks more sawtooth-like than sinusoidal.

V12: according to Soszyński et al. (2009a), this is RRL OGLE-LMC-RRLYR-05278 with period 0.5870247 day.

V19: has the magnitude and color of cluster  $\delta$  Sct, but its shape does not resemble a  $\delta$  Sct; therefore, we classify it as unknown type.

V25: this is a very faint source for which we do not have psf photometry, and therefore the light curve cannot be transformed into magnitudes. We originally classified this variable as  $\delta$  Sct based on its shape and period, but its position in the *HST* CMD (Figure 6) reveals it is more likely an eclipsing binary.

V34: another very faint source, for which we lack color information. Its light curve resembles a  $\delta$  Sct more than an eclipsing binary; therefore, it is probably a background source.

V41: according to Soszyński et al. (2009a), this the RRe (second-overtone pulsator) OGLE-LMC-RRLYR-05379 with a period of 0.272447 day.

V48: this is OGLE-LMC-RRLYR-05394 from Soszyński et al. (2009a), with period 0.472163 day.

V49: even though it has a magnitude and color that puts it right at the MSTO, its period is much longer than the time span of the observations. Even though it could be a  $\delta$  Sct with a very long period, it is more likely a background RRL that was not discovered by OGLE.

V50: another source without color. The shape of light curve and period indicate a  $\delta$  Sct, although its faintness implies a background source. With  $A_r = 0.5$ , it is one of the variables with the largest amplitudes in the sample.

V52: has the color of a  $\delta$  Sct, but a much fainter magnitude, probably a background  $\delta$  Sct.

V53: a  $\delta$  Sct appearing about a magnitude below the MSTO. It is most likely an LMC field  $\delta$  Sct somewhat on the background.

V55: another variable too faint in  $g$  to obtain a color. It is very faint in  $i$ , but has an amplitude  $\sim 0.5$  mag. Its light curve shape resembles a  $\delta$  Sct and an RRL, but we cannot adventure any firm classification.

V56: Most probably a long-period eclipsing binary.

V57: similar to V53.

V59: the brightest of all variables, but with a very small amplitude to be an RRL. We cannot determine a classification for this variable.

V60: too faint and red to be a  $\delta$  Sct. We set its class as unknown.

V61: has the right magnitude and color to be a  $\delta$  Sct in NGC 1846, but its very high amplitude and rather long period points at a background RRL.

V64: is one of the bluest variables in the sample. Brighter than the MSTO, its partial light curve resembles the sinusoidal shape of an RRc, although that would be a very tentative classification.


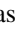

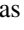
V68: like V53 and V57, this variable appears below the MSTO of NGC 1846. Is probably a background  $\delta$  Sct.

V70: the partial shape of this light curve hints at a background RRL.

V72: same as V52.

V75: another variable for which we could not transform relative flux into magnitudes. Its short period and light curve shape indicate is a  $\delta$  Sct.

### ORCID iDs

R. Salinas  <https://orcid.org/0000-0002-1206-1930>  
 A. K. Vivas  <https://orcid.org/0000-0003-4341-6172>  
 J. Strader  <https://orcid.org/0000-0002-1468-9668>  
 R. Contreras Ramos  <https://orcid.org/0000-0001-7948-9731>

### References

- Alard, C. 2000, *A&AS*, **144**, 363  
 Andersen, M. F., Arentoft, T., Frandsen, S., et al. 2009, *CoAst*, **160**, 9  
 Bastian, N., & de Mink, S. E. 2009, *MNRAS*, **398**, L11  
 Bastian, N., & Niederhofer, F. 2015, *MNRAS*, **448**, 1863  
 Bastian, N., & Silva-Villa, E. 2013, *MNRAS*, **431**, L122  
 Baumgardt, H., Parmentier, G., Anders, P., & Grebel, E. K. 2013, *MNRAS*, **430**, 676  
 Brandt, T. D., & Huang, C. X. 2015, *ApJ*, **807**, 25  
 Breger, M. 2000, in ASP Conf. Ser. 210, *Delta Scuti and Related Stars*, ed. M. Breger & M. Montgomery (San Francisco, CA: ASP), 3  
 Catelan, M., Minniti, D., Lucas, P. W., et al. 2013, 40 Years of Variable Stars: A Celebration of Contributions by Horace A. Smith, ed. K. Kinemuchi et al., 139, arXiv:1310.1996  
 Correnti, M., Goudfrooij, P., Puzia, T. H., & de Mink, S. E. 2015, *MNRAS*, **450**, 3054  
 Epanchikov, V. A. 1969, *Teor. Veroyatnost. i Primenen*, **14**  
 Girardi, L., Eggenberger, P., & Miglio, A. 2011, *MNRAS*, **412**, L103  
 Goudfrooij, P., Girardi, L., & Correnti, M. 2017, *ApJ*, **846**, 22  
 Goudfrooij, P., Girardi, L., Rosenfield, P., et al. 2015, *MNRAS*, **450**, 1693  
 Goudfrooij, P., Puzia, T. H., Kozhurina-Platais, V., & Chandar, R. 2009, *AJ*, **137**, 4988  
 Grocholski, A. J., Cole, A. A., Sarajedini, A., Geisler, D., & Smith, V. V. 2006, *AJ*, **132**, 1630  
 Hook, I. M., Jørgensen, I., Allington-Smith, J. R., et al. 2004, *PASP*, **116**, 425  
 Kaluzny, J., & Rucinski, S. M. 2003, *AJ*, **126**, 237  
 Keller, S. C., Mackey, A. D., & Da Costa, G. S. 2011, *ApJ*, **731**, 22  
 King, I. 1962, *AJ*, **67**, 471  
 Li, C., de Grijs, R., & Deng, L. 2014, *ApJ*, **784**, 157  
 Mackey, A. D., & Broby Nielsen, P. 2007, *MNRAS*, **379**, 151  
 Mackey, A. D., Broby Nielsen, P., Ferguson, A. M. N., & Richardson, J. C. 2008, *ApJL*, **681**, L17  
 Milone, A. P., Bedin, L. R., Piotto, G., & Anderson, J. 2009, *A&A*, **497**, 755  
 Milone, A. P., Marino, A. F., D'Antona, F., et al. 2017, *MNRAS*, **465**, 4363  
 Niederhofer, F., Hilker, M., Bastian, N., & Silva-Villa, E. 2015, *A&A*, **575**, A62  
 Piatti, A. E., Keller, S. C., Mackey, A. D., & Da Costa, G. S. 2014, *MNRAS*, **444**, 1425  
 Pietrinferni, A., Cassisi, S., Salaris, M., & Castelli, F. 2004, *ApJ*, **612**, 168  
 Poleski, R., Soszyński, I., Udalski, A., et al. 2010, *AcA*, **60**, 1  
 Soszyński, I., Udalski, A., Szymański, M. K., et al. 2009a, *AcA*, **59**, 239  
 Stellingwerf, R. F. 1978, *ApJ*, **224**, 953  
 Stetson, P. B. 1987, *PASP*, **99**, 191  
 Stetson, P. B. 1993, in IAU Coll. 136, *Stellar Photometry—Current Techniques and Future Developments*, ed. C. J. Butler & I. Elliott (Cambridge: Cambridge Univ. Press), 291  
 Stetson, P. B. 1994, *PASP*, **106**, 250  
 Taylor, M. B. 2006, in ASP Conf. Ser. 351, *Astronomical Data Analysis Software and Systems XV*, ed. C. Gabriel et al. (San Francisco, CA: ASP), 666  
 Tody, D. 1986, *Proc. SPIE*, **627**, 733  
 Tody, D. 1993, in ASP Conf. Ser. 52, *Astronomical Data Analysis Software and Systems II*, ed. R. J. Hanisch, R. J. V. Brissenden, & J. Barnes (San Francisco, CA: ASP), 173  
 Vivas, A. K., & Mateo, M. 2013, *AJ*, **146**, 141  
 Yang, W., Bi, S., Meng, X., & Liu, Z. 2013, *ApJ*, **776**, 112